Determination of Helium-Discharge Atmospheric-Pressure Plasma Parameters and Distribution Using Numerical Simulation*)

Kladphet THANET, Wannakuwaththawaduge T. L. S. FERNANDO, Kazumasa TAKAHASHI[1)], Takashi KIKUCHI[1,2)] and Toru SASAKI[1)]

Department of Energy and Environment Science, Nagaoka University of Technology, Nagaoka 940-2188, Japan
[1)]*Department of Electrical, Electronics and Information Engineering, Nagaoka University of Technology, Nagaoka 940-2188, Japan*
[2)]*Department of Nuclear System Safety Engineering, Nagaoka University of Technology, Nagaoka 940-2188, Japan*

(Received 11 November 2020 / Accepted 24 February 2021)

This study investigated the chemical distribution of an atmospheric-pressure plasma jet (APPJ) along its propagation direction using numerical simulation. Low-resolution spectral data were used to estimate the gas temperature and the excitation temperature. These estimations were used with a collisional-radiative model to elucidate population densities and the electron temperature. A global model was applied to investigate the chemical species distribution in the plasma jet. The thermodynamic properties of the APPJ corresponded well to the relation $T_g < T_{exc} < T_e$ for all the positions along the jet propagation. Chemical species generation and propagation along the plasma jet were numerically simulated using the GM with input parameters derived from the CR model and the ideal gas law.

Keywords: atmospheric-pressure plasma, numerical modeling, chemical species distribution, spectral characterization

DOI: 10.1585/pfr.16.2401060

1. Introduction

Atmospheric-pressure plasma (APP) has attracted considerable attention owing to its applicability in a wide range of environmental, chemical, biomedical, and material processes [1–5]. The non-thermal properties of APP are suitable for temperature-sensitive applications. Chemical species generation through APP also increases its potential use in applications such as surface treatment, sterilization, and nanoparticle synthesis. Generation of APP jets (APPJs) using dielectric or metal capillaries has been widely studied in the biomedical and material-processing fields because of its feasibility in plasma patterning for surface treatments and focusing APP to a local position [6–10]. Although APPJ properties are important to their applications, their qualitative properties are difficult to study from experimental observations. Therefore, numerical modeling is used to predict the properties of APP [11–15].

The behavior of APPJs is important for understanding thermodynamic properties including gas temperature (T_g), rotational temperature (T_{rot}), excitation temperature (T_{exc}) and electron temperature (T_e) in the plasma [16–19]. Optical emission spectroscopy (OES) is a widely used technique to investigate such properties using experimental observations [20–23]. The accuracy of estimating such thermodynamic properties varies with the resolution of the obtained OES [24–27]. APPs are known to be derived from non-local thermodynamic equilibrium conditions to non-equilibrium between the rotational temperature T_{Rot}, the excitation temperature T_{exc}, and the electron temperature T_e. The rotational temperature T_{Rot} provides information about the gas temperature T_g. The use of OH lines or the second positive systems of N_2 (C–B, 0–0, or 0–2) are widely used techniques to estimate T_g using OES information [28–30]. Furthermore, the use of intensity of working gas or stark broadening can be used to estimate T_{exc} and T_e, respectively [31,32]. However, estimation of these thermodynamic properties using OES requires a high-resolution spectrometer. Other than the use of high-resolution spectrometers, T_g and T_{exc}, which are estimated from the excitation level population, can be used with a collisional radiative (CR) model to estimate T_e [33–36]. The distribution of the chemical species along APPJs provides vital information to improve their applicability. Experimental investigations of these chemical distributions can be performed using the localized OES of the plasma jets. However, the determination of such properties is a challenging process. Therefore, numerous studies have used numerical modeling to predict the possible chemical distributions along APPJs [12, 15, 37–39]. A global model (GM) is one of the modeling techniques widely used to estimate the time evolution of chemical species of APPJs [37–40].

In this study, we focused on investigating the ther-

author's e-mail: thanet@stn.nagaokaut.ac.jp
*) This article is based on the presentation at the 29th International Toki Conference on Plasma and Fusion Research (ITC29).

modynamic behaviors and chemical species distributions along APPJs using a CR model and GM. Optical emission lines collected from a double-electrode configured APPJ were used with a general approach on N_2 (C–B, 0–0) lines to estimate T_g. The excitation temperature (T_{exc}) describes the population of atomic excited states assuming that this follows a Boltzmann distribution. Considering the degeneracy of each atomic state, the population come by [18, 19, 41], and the CR model was applied to estimate the relations between the thermodynamic properties of APPJs. The distribution of chemical species along the direction of plasma jet propagation was estimated numerically using the GM.

2. Numerical Modeling Methodology

2.1 CR model with atomic collisions

Optical emission spectra provide information about the atomic process in excited atoms. These experimental observations with numerical simulations can provide details about the plasma parameters. To analyze such processes, the population of excited levels in the working gas of APP must be estimated. For such work, CR models, which were first introduced by Bates *et al.* [42, 43], and Johnson *et al.* [44], have been extensively used.

In CR models, rate equations are written for the modeled energy levels of atoms or ions, and various processes that affect the excited and de-excited electron number density of the modeled levels are simulated. Therefore, in CR models the population number densities of the ground state and modeled excited states are calculated along with the free electron density [22, 35, 45–47]. However, to generate the APPJs inter-atomic collision is important rather than the free electron collision. In this study, the noble gas helium was introduced into the equipment. The collected localized optical emission lines were used to estimate the propagation of T_g and T_{exc} with the plasma jet. Estimated values were input into the CR model to calculate the T_e and population number densities of the helium gas.

As an APPJ is considered to be a weakly ionized plasma, the population number densities of the excited level N_p (where $p \geq 2$; $p = 1$ corresponds to the ground state) were approximately estimated using the CR model as shown in Eq. (1):

$$\frac{dN_p}{d_t} = C_{1p}N_eN_1 + N_1\sum_{j=1,j\neq p}^{M} K_{jp}N_j - N_pN_1\sum_{i=1,i\neq p}^{M} K_{pi} = 0, \quad (p \geq 2) \tag{1}$$

where M is the upper limit of the excitation level included in the CR model. The matrix and vectors are defined as follows:

$$\overline{K}\begin{pmatrix} \sum_{j=1,j\neq 2}^{M} K_{2j} & -K_{32} & \cdots & -K_{M2} \\ -K_{23} & \sum_{j=1,j\neq 3}^{M} K_{3j} & \cdots & -K_{M3} \\ \vdots & \vdots & \ddots & \vdots \\ -K_{2M} & -K_{3M} & \cdots & \sum_{j=1}^{M-1} K_{Mj} \end{pmatrix}, \tag{2}$$

$$N = \begin{pmatrix} N_2 \\ \vdots \\ N_M \end{pmatrix}, \tag{3}$$

$$C_1 = \begin{pmatrix} C_{12} \\ \vdots \\ C_{1M} \end{pmatrix}, \tag{4}$$

$$K_1 = \begin{pmatrix} K_{12} \\ \vdots \\ K_{1M} \end{pmatrix}. \tag{5}$$

For the excited-state number density $N_p = (p = 2, 3, 4, \cdots M)$, we rewrite Eq. 1 as

$$\overline{K}N = N_eC_1 + N_1K_1. \tag{6}$$

We know that the electron temperature of the plasma and gas temperature are considered in Kelvin, and that theelectron temperature is much higher than the gas temperature. For most problems in plasma, the atomic collision excitation from the ground state is basically negligible. Hence,

$$N_eC_{1p} \gg N_1K_{1p}, \tag{7}$$

and Eq. 6 can be approximated to

$$\overline{K}N = N_eC_1. \tag{8}$$

However, we must confirm the steadiness of the matrix $\overline{K}$ in Eq. 2. The collisional de-excitation from the level p to the ground state K_{p1} in the ground state in the summation of diagonal elements is negligibly small in general. If the diagonal element does not include K_{p1}, the matrix $\overline{K}'$ becomes always singular for any matrix elements. Then the summation of every row vector in the matrix becomes exactly a zero vector. Fortunately, owing to the addition of the term K_{p1} into the summation of each diagonal element in Eq. 2, $\overline{K}$ generally becomes a regular matrix. Furthermore, for low-gas-temperature conditions, the atomic collisional de-excitation to the ground state K_{p1} ($j \neq 1$) cannot be neglected. Thus, we always have an algebraic solution of the vector N from Eq. 8. Hence,

$$N = N_e\overline{K}^{-1}C_1, \tag{9}$$

where the matrix $\overline{K}^{-1}$ depends only on T_g and the vector C_1 only on T_e. The gas temperature has almost been studied by the rotational temperature in APPs [28, 29]. Even in pure helium plasma, we can detect molecular band spectra

Table 1 Atomic data of helium gas.

Level number p	Designation	Term	J	Excitation Energy $\varepsilon_{1p}(eV)$	Statistical weight g_p
1	*1s2*	*1S*	0	0.0000	1
2	*1s.2s*	*3S*	1	19.8196	3
3	*1s.2s*	*1S*	0	20.6158	1
4	*1s.2p*	*3P*	2	20.9641	9
5	*1s.2p*	*1P*	1	21.2180	3
6	*1s.3s*	*3S*	1	22.7184	3
7	*1s.3s*	*1S*	0	22.9203	1
8	*1s.3p*	*3P*	2	23.0070	9
9	*1s.3d*	*3D*	3	23.0736	15
10	*1s.3d*	*1D*	2	23.0740	5
11	*1s.3p*	*1P*	1	23.0870	3
12	*1s.4s*	*3S*	1	23.5939	3
13	*1s.4s*	*1S*	0	23.6735	1
14	*1s.4p*	*3P*	2	23.7078	9
15	*1s.4d*	*3D*	3	23.7360	15
16	*1s.4d*	*1D*	2	23.7363	5
17	*1s.4f*	*3F*	3	23.7370	21
18	*1s.4f*	*1F*	3	23.7371	7
19	*1s.4p*	*1P*	1	23.7420	3
20	*1s.5s*	*3S*	1	23.9719	3
21	*1s.5s*	*1S*	0	24.0112	1
22	*1s.5p*	*3P*	2	24.0282	9
23	*1s.5d*	*3D*	3	24.0426	15
24	*1s.5d*	*1D*	2	24.0428	5
25	*1s.5f*	*3F*	3	24.0431	21
26	*1s.5f*	*1F*	3	24.0431	27
27	*1s.5g*	*3G*	4	24.0432	9
28	*1s.5g*	*1G*	4	24.0432	3
29	*1s.5p*	*1P*	1	24.0457	3
30	*1s.6s*	*3S*	1	24.1689	1

such as a second positive system of N_2 molecule transition. In the next step, we fixed the gas temperature and used the relation of the excitation temperature from the experimental result to determine the electron temperature using Eq. 10:

$$\frac{N_p}{N_q} = \frac{\sum_{i=1}^{M}[\overline{K}^{-1}(T_{\mathrm{g}})]_{pi}C_{1i}(T_{\mathrm{e}})}{\sum_{i=2}^{M}[\overline{K}^{-1}(T_{\mathrm{g}})]_{qj}C_{1j}(T_{\mathrm{e}})} = F(T_{\mathrm{g}}, T_{\mathrm{e}}). \quad (10)$$

We found the value of the gas temperature and subsequently could derive the electron temperature by spectroscopic analysis of the excitation temperature together with the CR model calculation. From the CR model, we estimated the population number density of helium in this study by using the atomic data of helium provided in Table 1 from the atomic spectra database of the National Institute of Standards and Technology [48].

2.2 Global model

To comprehend the chemical reactive species in APPs, zero-dimensional plasma chemical kinetics simulations such as GMs are widely used [49], as the chemical species generated through APPJs play a major role in improving the applicability of such techniques. This study also considered the use of GM to estimate the behaviors of the chemical species along the APPJs. The obtained results were compared with experimentally observed results.

For this work, we considered 25 main species, as listed in Table 2, and 56 possible reactions were adopted from the work by Murakami *et al.* [39] for the numerical simulation. Our numerical simulation was carried out in time dependent model. It assumed that the plasma moves by the constant drift velocity determined by the introduced gas flow. The governing rate equation considered in this study is expressed as follows:

Table 2 List of species.

		List of species
Neutral species	Carrier gas	He
	Humidity air	N_2 (~78%), O_2 (~21%), H_2O (variable)
	Reactive species	He^*, H, OH, O, O_3, N, NO, NO_2
Ions	Positive	He^+, O^+, O_2^+, N^+, N_2^+
	Negative	H^-, OH^-, O^-, O_2^-, O_3^-, NO^-, NO_2^-
Electron		Electron (e^-)

$$\frac{dn_i}{dt} = n_i \sum_{j=1}^{25} k_{ij} n_j + n_i \sum_{j=1}^{25}\sum_{m=1}^{25} k_{ijm} n_j n_m + R_{\mathrm{ex}}, \quad (11)$$

where t, n_i, k_{ij}, k_{ijm} and R_{ex} denote time, number density of i_{th} species, two-body reaction rate for i and jth species, three- body reaction rate for i, j and mth species and external rate source term, respectively [14, 39, 50].

Even though the GM predicts the time evolution of chemical species, this study considered the position evolution of chemical species to understand the distribution of such species along a plasma jet. To convert the time evolution to position evolution, we considered the flow behavior of the APPJ in the laminar regime and estimated the laminar flow velocity to estimate the propagation time and position, as follows:

$$\frac{1}{\tau} = \frac{v_l}{d}. \quad (12)$$

Where τ is the time considered in the time evolution estimation in the GM, v_l is the laminar flow velocity of the plasma jet and which is 42.26 m/s is given by the experimentally obtained from the gas flow rate considering with the cross-section of the tube [10, 51], and d is the position corresponding to the relevant time evolution. We assumed that the flow velocity of the plasma was constant in the calculation.

3. Results and Discussion

3.1 Thermodynamic parameter estimation using low-resolution spectroscopy

OES provides important information on the thermodynamic properties of APPJs. The gas and excitation temperatures are the thermodynamic properties widely explained using experimentally obtained OES. In this study, we also estimated the above thermodynamic properties using experimentally obtained OES. The spectra were obtained in the range of 200 - 800 nm using a spectrometer system (HAMMAMATSU: PMA-12) with a spectral resolution $\Delta\lambda < 2$ nm.

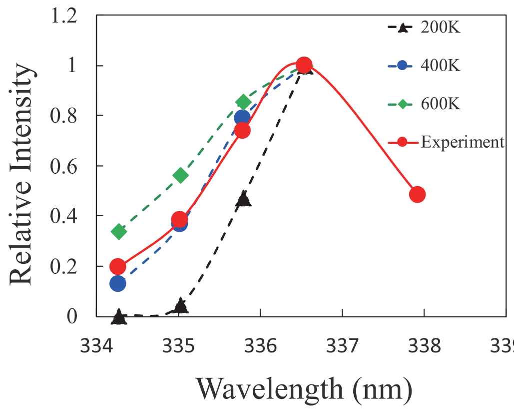

Fig. 1 Determination of gas temperature from synthetic spectra for the N_2 (C–B, 0–0)transition.

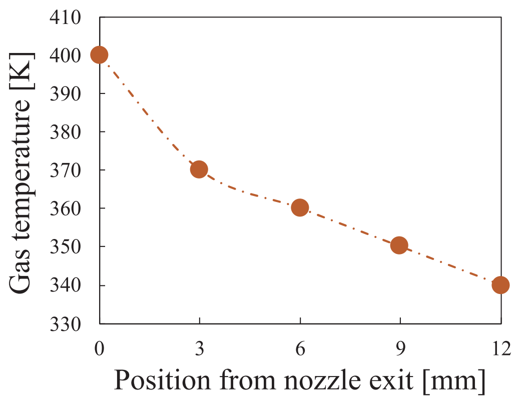

Fig. 2 Gas temperature estimated by synthetic spectrums for the N_2 (C–B, 0–0) transition alongthe plasma jet.

The gas temperature T_g can be estimated directly using high-resolution OES from the rotational temperature T_{Rot}. Although low-resolution OES was mainly used to detect the possible radicals and emission lines of the plasma, this study estimated T_g using averaging of summing of theoretical intensities over the experimentally detected lines from the equilibrium between the gas temperature T_g and the rotational temperature T_{rot}.

The nitrogen second positive system N_2 ($C^2\Pi_u \rightarrow B^3\Pi_g$, 0–0) 337 nm line is the commonly used emission line system to estimate the rotational temperature or T_g of the plasma state [28, 29, 52]. In this work, N_2 (C–B, 0–0) simulated values were summed and averaged over the spectrum around $\lambda \pm (\Delta\lambda/2)$ of the experimentally obtained OES lines. The relative intensities of these values were then considered and fitted by a least-squares method along the experimentally obtained OES spectrum for an absolute T_{rot} value. The gas temperature was changed and proceeded further until the simulated shape closely coincided with the experimental spectral curve, as shown in Fig. 1. The line broadening of the simulated fitting curve expands with the increase in gas temperature. The T_g value that most closely synthesized the experimental spectrum was considered the rotational temperature of the plasma state at that position.

This method was applied to estimate T_g along the direction of plasma jet propagation, and the distribution of T_g along the jet position is shown in Fig. 2. As shown in Fig. 2, T_g was approximately 400 K for the helium APPJ at the nozzle exit as possible expected values [53]. In addition, as the plasma jet propagated, T_g was also observed to decrease toward room temperature at the bottom of the plasma jet. In addition to T_g, the He excitation temperature can also be estimated using the low-resolution emission spectra. In this study, to determine T_{exc}, a Boltzmann plot was drawn with the quantity $\ln(I_{ij}/\lambda_{ij}g_i)$ against the energy of the corresponding energy of the He lines, where i and j are the upper and lower levels, respectively. Recorded correspondence intensities (I_{ij}) and wavelength (λ_{ij}) were used with the Einstein coefficient (A_{ij}) and statistical weight (g_i) obtained from the National Institute of Standards and Technology (NIST) [48]. He spectra of 389, 471, 587, 667, 706, and 728 nm were used to calculate T_{exc}, and the information related to each line is listed in Table 3.

Table 3 Excitation energy and transition strength of helium.

(nm) Wave-length	Configuration [48] Upper level	Lower level	Energy (eV) [48] Upper level	Lower level	Einstein A Coeff. A_{ij} (1/s)	Lifetime
389	1s3p ^{3}P	1s2s ^{3}S	23.0071	19.8196	9.47E+6	106 ns
471	1s4s ^{3}S	1s2p ^{3}P	23.5939	20.9641	3.17E+6	315 ns
587	1s3d ^{3}D	1s2p ^{3}P	23.0737	20.9641	4.20E+7	23 ns
667	1s3d ^{1}D	1s2p ^{1}P	23.0741	21.2180	2.12E+7	47 ns
706	1s3s ^{3}S	1s2p ^{3}P	22.7185	20.9641	9.28E+6	108 ns
728	1s3s ^{1}S	1s2p ^{1}P	22.9203	21.2180	1.83E+7	54 ns

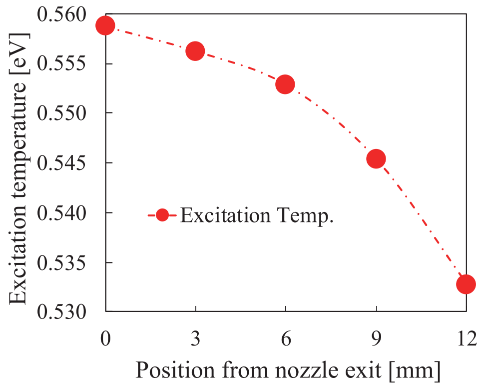

Fig. 3 Excitation temperature distribution along the plasma jet.

Using the localized OES data with the Boltzmann plot method, T_{exc} was estimated along the direction of plasma jet propagation, as shown in Fig. 3. T_{exc} is high at the nozzle exit and tends to decrease as the jet propagates. Such behavior along the plasma jet can be expected as the relaxation of rotational levels and metastable excited levels of helium decrease.

3.2 Estimation of population number density, electron temperature, and electron density

Electron density and electron temperature are important parameters that describe the plasma state. Akatsuka *et al.* [22, 35] explained the probability of population density in argon plasma with the presence of excited-level populations and excitation kinetics of nonequilibrium ionizing argon discharge plasma at atmospheric pressure [22, 35]. Estimating the parameters of n_e and T_e using the low-resolution emission line spectra is a difficult process. Therefore, in this study, as we were able to estimate T_g and T_{exc} using the experimentally obtained OES data, the CR model was adopted to estimate the T_e and population densities of the working gas. The estimated T_{exc} along the plasma jet in this study fell in the range 0.51 - 0.57 eV and, according to the CR model, these values relate to low electron temperature values. Analysis of the relationship between the lower electron temperature and excitation was carried out in this work. For this purpose, we consider the relation between the thermodynamic properties T_g, T_{exc}, and T_e in the CR model, as shown in Fig. 4.

The electron temperature for certain T_{exc} and T_g was estimated using this method to understand its propagation along the plasma jet. Figure 5 shows the propagation of T_{exc} and T_e along the plasma jet for the corresponding T_g at each position.

Although the electron temperature decreases along the direction of jet propagation, the relation between the gas temperature, excitation temperature, and electron temperature maintains the condition of $T_g < T_{exc} < T_e$ along the direction of jet propagation. This information confirms that the considered plasma jet maintains its non-equilibrium condition along the plasma jet.

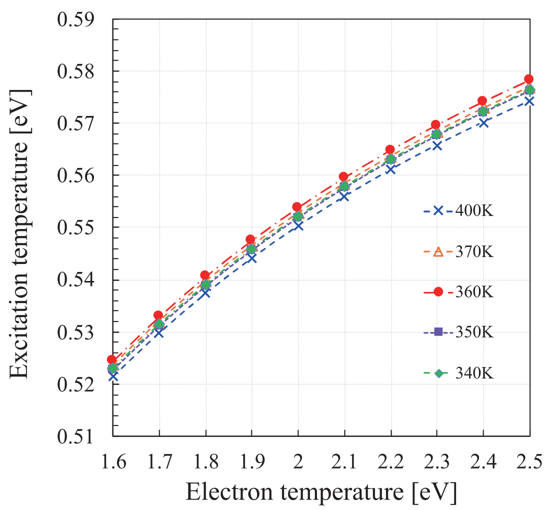

Fig. 4 Calculation of excitation temperature as a function of electron temperature from the CR model with level pairs at $n_e = 10\,\mathrm{cm}^{-3}$, $T_g = 340$ - $400\,\mathrm{K}$ at $P = 1$ atm as a function of electron temperature.

Many studies have estimated the electron densities of helium plasma in APPJs using the stark broadening method [3, 4]. As our OES system has low resolution, this study used the CR model to numerically estimate the population number density for helium excited states. In addition, this study used the relation between the electron density and population density state in Eq. (9) to estimate the electron number density for this simulation.

According to the CR model estimations, the relation between T_e and n_e shows a similar shape for different electron densities against electron temperature, as shown in Fig. 6. However, the curves shift to higher values as the electron density increases. Using the information from the helium excited energy level states in Table 1, the population number density of each level was numerically estimated using the CR model against T_e, as shown in Fig. 7. For this numerical estimation, experimentally obtained T_e and T_g values for the plasma jet at the nozzle exit were used with the CR model at an electron density of $10^{11}\,\mathrm{cm}^{-3}$. Ex-

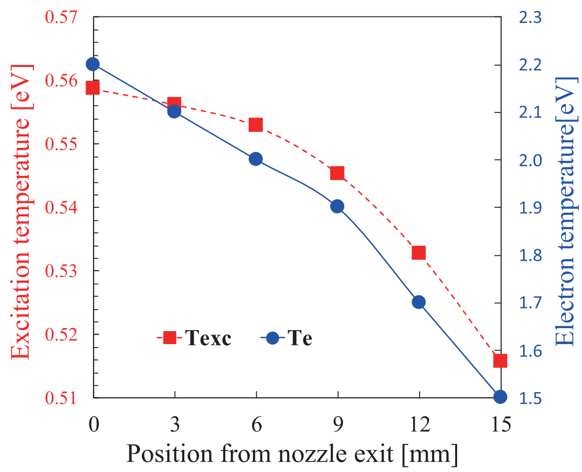

Fig. 5 CR model calculation of the distribution of excitation and electron temperatures along the plasma jet.

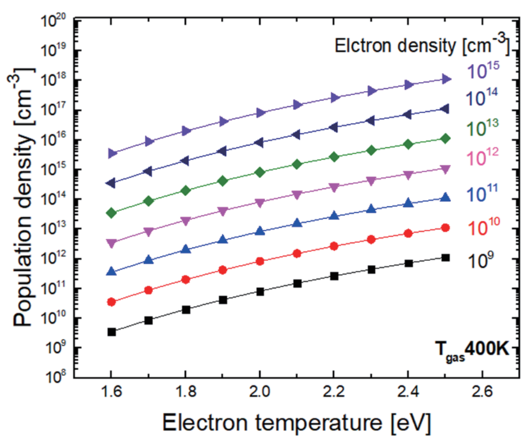

Fig. 6 Shows the relation between the He* density as a function of the different from 10^9 to $10^{15}\,\mathrm{cm}^{-3}$ electron density with $T_g = 400\,\mathrm{K}$.

perimental evidence of electrons density for helium APPJs tends to be around 10^{11} cm^{-3} [39]. According to the model calculation, the triplet states of the helium energy levels show higher population densities compared to the singlet states. Therefore, the emission lines between triplet states should have high intensity compared to the singlet transitions. Experimental work conducted by Fernando *et al.* [10, 51], parallel to this study, confirmed that triplet transitions have the highest emission intensities for He plasma. Using the estimated thermodynamic profiles along the plasma jet with the CR model, this study numerically estimated the population number density distribution, as shown in Fig. 8. Figure 8 clearly shows a decrease in the excited level population number densities as the plasma jet propagates. As per our experimental observations, we also noted that the intensity of the helium emission lines decreased along the plasma jet [10, 51]. This can be identified as helium excited atoms tending to relax as the APPJ propagates. As per the CR model, the population density strongly depends on the electron temperature.

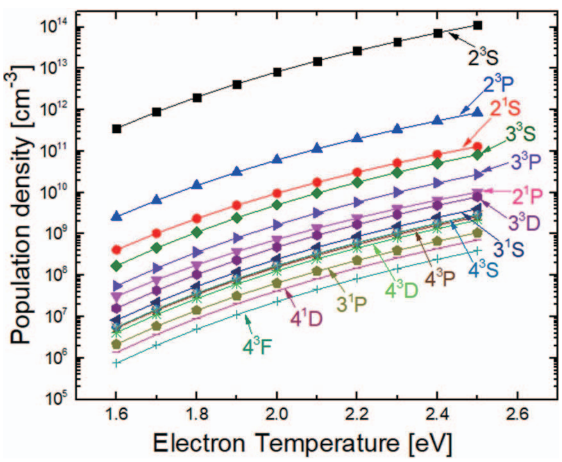

Fig. 7 GM estimate of helium population density as a function of electron temperature at $n_e = 10\,\mathrm{cm}^{-3}$, $T_g = 400$ K at $P = 1$ atm.

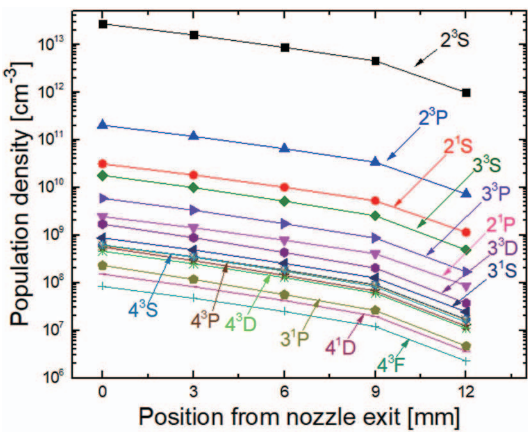

Fig. 8 Estimate of helium population density against position of APPJ from the nozzle exit along the plasma jet.

3.3 Estimation of chemical distribution along the APPJ

We used a GM to numerically simulate the distribution of chemical species along the jet propagation. The GM described by Murakami *et al.* [39] was considered and numerically simulated using the initial and estimated parameters. The population density of excited level $2p^3$P, which was estimated for an electron density of 10^{11} cm^{-3}, was used as the initial condition of excited helium density as per the CR model estimation and observed emission lines. The time evolution estimation was converted to the position evolution using Eq. (11) to describe the behavior of the chemical species distribution along the plasma jet. The estimation of chemical species was also focused mainly on the above-mentioned radical estimation. For this purpose, the initial input parameters of electron density and densities of the chemical species of helium, nitrogen, oxygen, and H_2O ppm were estimated considering the atmospheric conditions of the experiment. The chemical species distribution along the plasma jet was numerically simulated using the aforementioned parameters using the GM. The distribution of species along the plasma jet is shown in Figs. 9 - 11.

As illustrated in Figs. 9 - 11, the chemical species exhibit sudden generation around the nozzle exit before propagating along the plasma jet. The interaction of air with the helium plasma plume at the nozzle exit and nanosecond-scale reaction rate are the main reasons for the sudden increase in species at the nozzle exit.

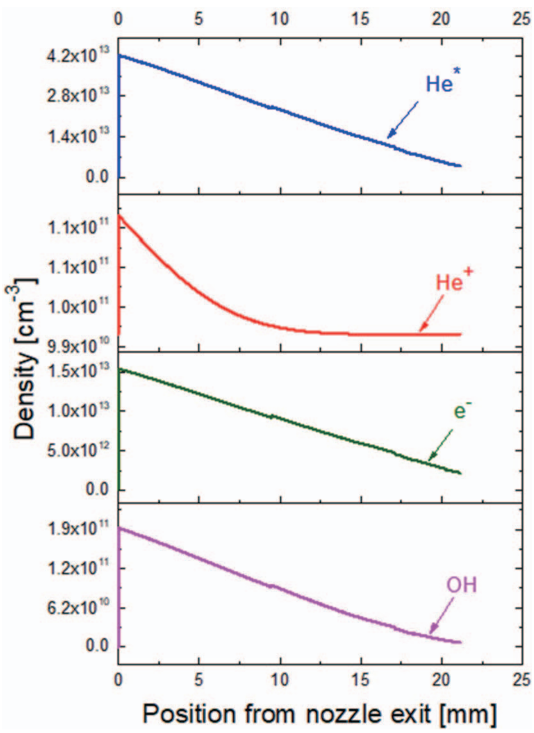

Fig. 9 Distribution of density of chemical species along the plasma jet estimated by the GM.

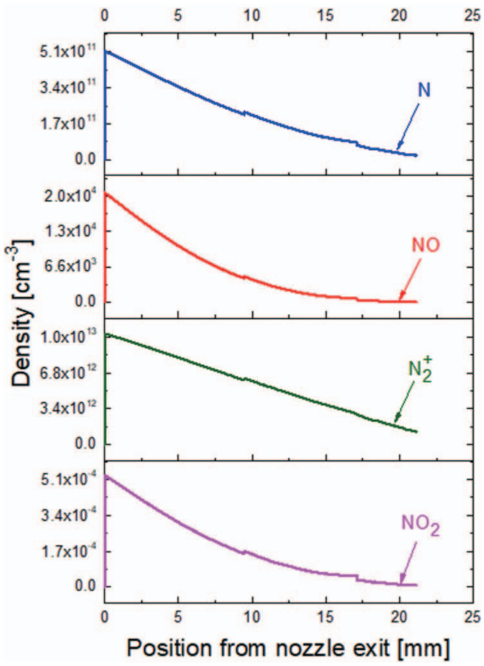

Fig. 10 Distribution of density of nitrogen chemical species along the plasma jet estimated by GM.

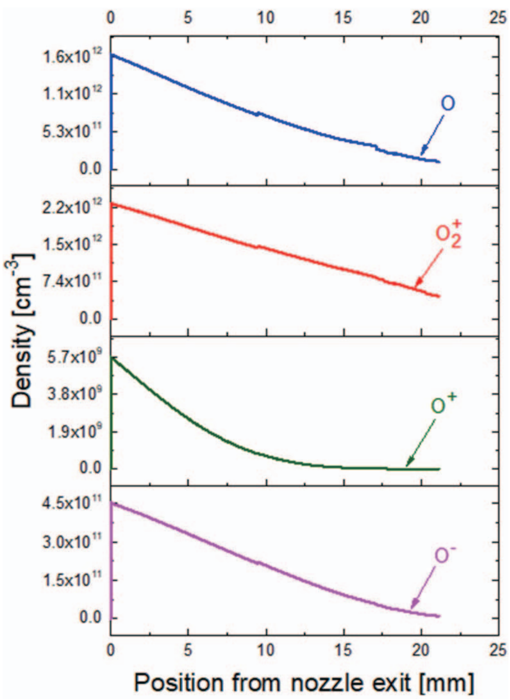

Fig. 11 Distribution of density of oxygen chemical species along the plasma jet estimated by GM.

Figure 12 illustrates the normalized distribution of chemical species around the nozzle exit. As the densities of chemical species are of different orders, the highest individual density value for the defined time scale was used to normalize the distribution of chemical species.

Although this study uses an electron density of

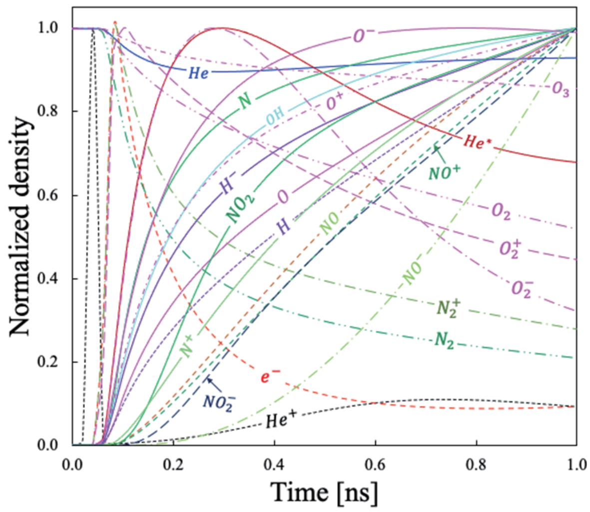

Fig. 12 Predictednormalized density of chemical specimens in the APPJ with ambient air.

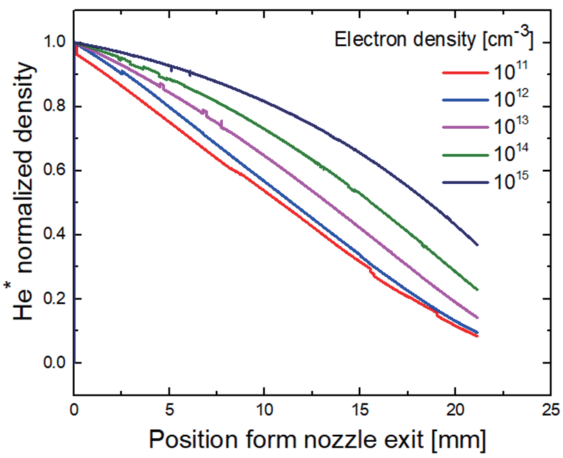

Fig. 13 Illustrate the behavior of normalized He* distribution along plasma jet.

10^{11} cm^{-3} as the initial condition, further investigation was performed to understand the behavior of chemical species in relation to electron density is shown in Figs. 13, 14. Figures 13 and 14 illustrate the behavior normalized He* and OH distribution as a function of the difference from 10^{11} to 10^{15} cm^{-3} electron density along with the plasma jet. The He* and OH density could be significant for using comparison with experiment work. This study will be the focus of our future study.

4. Conclusions

In this study, we investigated the behavior of APPJs through numerical modeling. Low-resolution spectroscopy data were used to estimate the gas temperature and the excitation temperature was estimated along the jet propagation. As per the numerical estimation, the gas temperature was approximately 400 K at the nozzle exit and

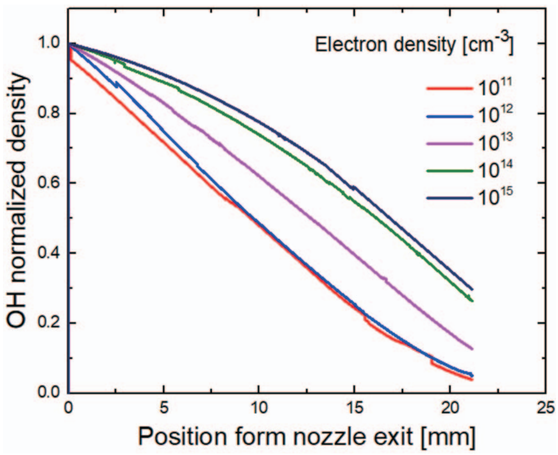

Fig. 14 Illustrate the behavior of normalized OH distribution along plasma jet.

decreased to room temperature as the jet propagated. The estimation of the excitation temperature showed a higher value at the nozzle exit with a tendency to reduce in value as the APPJ propagated.

The CR model for the helium working gas was used to estimate the electron temperature and population densities in relation to the position of the plasma jet with the experimentally obtained gas temperature and excitation temperature data [10]. The thermodynamic properties of the APPJ corresponded well to the relation $T_g < T_{exc} < T_e$ for all the positions along the jet propagation. Chemical species generation and propagation along the plasma jet were numerically simulated using the GM with input parameters derived from the CR model and the ideal gas law.

[1] F. Tochikubo *et al.*, Jpn. J. Appl. Phys. **53**, 046202 (2014).
[2] P.V. Thai *et al.*, J. Appl. Phys. **125**, 063303 (2019).
[3] P.V. Thai *et al.*, Mater. Res. Express **6**, 9 (2019).
[4] R. Brandenburg *et al.*, Contrib. Plasma Phys. **47**, 72 (2007).
[5] K.D. Weltmann *et al.*, Pure Appl. Chem. **82**, 1223 (2010).
[6] X. Lu *et al.*, Appl. Phys. Lett. **92**, 151504 (2008).
[7] J.Y. Kim *et al.*, Biosens. Bioelectron. **26**, 555 (2010).
[8] T. Yuji *et al.*, Jpn. J. Appl. Phys. **46**, 795 (2007).
[9] M. Okubo *et al.*, IEEE Trans. Ind. Appl. **41**, 891 (2005).
[10] W.T.L.S. Fernando *et al.*, IEEE TRPMS **4**, 108 (2019).
[11] Y.H. Choi *et al.*, Thin Solid Films **506**, 389 (2006).
[12] J. Jánský and A. Bourdon, Appl. Phys. Lett. **99**, 161504 (2011).
[13] P. Wang *et al.*, J. Appl. Phys. **100**, 0145012 (2006).
[14] K. Niemi *et al.*, Plasma Sources Sci. Technol. **20**, 055005 (2011).
[15] J. Jánský *et al.*, J. Phys. D: Appl. Phys. **44**, 335201 (2011).
[16] O. Motret *et al.*, J. Phys. D: Appl. Phys. **33**, 1493 (2000).
[17] Z.S. Chang *et al.*, Phys. Plasmas **19**, 073513 (2012).
[18] K. Yambe *et al.*, Phys. Plasmas **24**, 063512 (2017).
[19] S.H. Nam *et al.*, Bull. Korean Chem. Soc. **24**, 827 (2001).
[20] D. Mariotti *et al.*, J. Appl. Phys. **101**, 013307 (2007).
[21] Q. Xiong *et al.*, Plasma Sources Sci. Technol. **22**, 015011 (2013).
[22] H. Akatsuka, Adv. Phys. **4**, 1592707 (2019).
[23] Y.K. Lee *et al.*, J. Phys. D: Appl. Phys. **44**, 285203 (2011).
[24] P.J. Bruggeman *et al.*, Plasma Sources Sci. Technol. **23**, 023001 (2014).
[25] J.P. Pichamuthu *et al.*, J. Appl. Phys. **43**, 4562 (1972).
[26] B. Bai, H.H. Sawin and B.A. Cruden, J. Appl. Phys. **99**, 013308 (2006).
[27] C. Biloiu *et al.*, J. Appl. Phys. **101**, 073303 (2007).
[28] S.B. Bayram and M.V. Freamat, Am. J. Phys. **80**, 664 (2012).
[29] U. Fantz *et al.*, Plasma Sources Sci. Technol. **15**, S137 (2006).
[30] D. Xiao *et al.*, Phys. Plasmas **21**, 053510 (2014).
[31] H. Park and W. Choe, Curr. Appl. Phys. **10**, 1456 (2010).
[32] C. Perez *et al.*, Phys. Rev. A **44**, 6785 (1991).
[33] M. Itoh, T. Yabe and S. Kiyokawa, Phys. Rev. A **35**, 233 (1987).
[34] K. Sawada *et al.*, J. Plasma Fusion Res. **5**, 001 (2010).
[35] H. Akatsuka, Phys. Plasmas **16,** 043502 (2009).
[36] C.P. Ballance *et al.*, Phys. Rev. A **74**, 012719 (2006).
[37] T. Murakami *et al.*, Plasma Sources Sci. Technol. **22**, 045010 (2013).
[38] T. Murakami *et al.*, 42nd AIAA Plasma Dynamics and Lasers Conference (2011).
[39] T. Murakami *et al.*, Plasma Sources Sci. Technol. **22**, 015003 (2012).
[40] D.X. Liu *et al.*, Plasma Sources Sci. Technol. **19**, 025018 (2010).
[41] H.R. Griem, Principle of Plasma Spectroscopy. Cambridge, U.K.: Cambridge Univ. Press, 1997.
[42] D.R. Bates *et al.*, Proc. R. Soc. Lond. A **267**, 297 (1962).
[43] D.R. Bates *et al.*, Proc. R. Soc. Lond. A **270**, 155 (1962)
[44] L.C. Johnson and E. Hinnov, Phys. Rev. **187**, 143 (1969).
[45] J. Vlcek, J. Phys. D: Appl. Phys. **22**, 623 (1989).
[46] A. Yanguas-Gil *et al.*, Phys. Plasmas **11**, 5497 (2004).
[47] T. Fujimoto, J. Quant. Spectrosc. Radiat. Transf. **21**, 439 (1979).
[48] A. Kramida *et al.*, NIST-Atomic Spectra Database https://physics.nist.gov/asd. (2018).
[49] A. Hurlbatt *et al.*, Plasma Process. Polym. **14**, 1600138 (2017).
[50] J. Wei and C.D. Prater, Adv. Catal. **13**, 203 (1962).
[51] W.T.L.S. Fernando *et al.*, in XXXIV ICPIG & ICRP-10, ISBN 978-4-900986-19-0, (2019).
[52] B. Twomey *et al.*, Plasma Chem. Plasma Process. **31**, 139 (2010).
[53] K. Thanet *et al.*, in XXXIV ICPIG & ICRP-10, ISBN 978-4-900986-19-0, (2019).